Theory of manganite superlattices

Chungwei Lin and Andrew J. Millis
Department of Physics, Columbia University, 538 W. 120th Street, New York, New York 10027, USA
(Received 5 August 2008; published 7 November 2008)

A theoretical model is proposed for the (0,0,1) superlattice manganite system $(LaMnO_3)_n(SrMnO_3)_m$. The model includes the electron-electron, electron-phonon, and cooperative Jahn-Teller interactions. It is solved using a version of the single-site dynamical mean-field approximation generalized to incorporate the cooperative Jahn-Teller effect. The phase diagram and conductivities are calculated. The behavior of the superlattice is found to be a good approximation to be an average over the density-dependent properties of individual layers, with the density of each layer fixed by electrostatics.

DOI: 10.1103/PhysRevB.78.184405 PACS number(s): 75.47.Lx, 68.65.Cd, 73.40.−c

I. INTRODUCTION

An exciting recent development in materials science is the ability to fabricate atomically precise multilayer structures involving transition-metal oxides.[1–6] Multilayer structure based on simple semiconductors such as Si and GaAs or AlGaAs gives rise to wide range of striking physical phenomena, such as the integer and fractional quantum Hall effects,[7,8] and are important for many classes of devices. It is therefore natural to expect that transition-metal oxides, which display a far richer variety of phenomena than do semiconductors,[9] will, in heterostructure form, yield an even more diverse set of new phenomena.

The colossal magnetoresistance (CMR) rare-earth manganites $La_{1-x}Sr_xMnO_3$ have been studied intensively[10–15] and have provided an important model system. These compounds display a wide range of phases with characteristic orbital, magnetic, and transport signatures,[10,11,16,17] providing opportunities both for creating many effects in the superlattice (SL) context and for detecting phases that may be created. Manganite superlattices have now been fabricated and are being studied experimentally[4–6] but have not yet received much theoretical attention. In this paper we present a theoretical analysis of these interesting systems. Our findings may be summarized by the following four rules: (1) the layer *charge distribution* mainly depends on the electrostatic interaction and has very weak dependence on the temperatures and on whether or not the system has orbital or magnetic order; (2) once the layer charge distribution is given, the *orbital order* at each layer is essentially determined by the bulk behavior at the same density: the propagation length of the orbital order along the superlattice is less than a lattice constant; (3) the interlayer *magnetic coupling* is ferromagnetic (FM) except between layers with densities close to one, where it is antiferromagnetic (AFM); and (4) the *in-plane conductivity* is essentially the average of *bulk* conductivities for the given layer charge distribution. These results indicate that the main effect of superlattice structure is simply to produce a layer-dependent charge distribution. Once the layer densities are known, each layer behaves basically according to the bulk phase diagram for that density with only weak proximity effects.

The rest of this paper is organized as follows. First we define the superlattice and discuss the interactions considered in the bulk model then we present and discuss results for a particular superlattice consisting of four layers of $LaMnO_3$ and one of $SrMnO_3$ in detail. From these and related calculations we infer the rules outlined above. Finally we use the rules to discuss recent experiments[4,5] arguing that the data still may not be displaying intrinsic behavior. We propose experiments on a variant of the superlattice which may be more definitive.

II. DEFINITIONS, HAMILTONIAN, METHODS, AND PHASES

A. Definition of superlattice

The high-temperature structure of $LaMnO_3$ is a slightly distorted version of the ABO_3 perovskite. It may be thought of as a simple-cubic lattice with Mn on the cube vertices and La in the body centers. The superlattices of interest here are composed of the same cubic lattice of Mn, with a superstructure defined by a periodic replacement of La by Sr. To specify the superlattice we must specify the direction along which the La or Sr sites alternate and the way the La and Sr ions are arranged. We will consider a (0,0,1) $(LaMnO_3)_m(SrMnO_3)_n$ superlattice, abbreviated as LmSn or (m,n), defined by m La planes perpendicular to the (0,0,1) cube axis, and followed by n Sr planes. The entire structure has a periodicity $(m+n)$ in the z (coordinate) direction while maintaining the original lattice translational symmetry in x and y. The upper panel of Fig. 1 shows a L4S1 (4,1) superlattice. We shall refer to each x-y plane as a layer.

B. Hamiltonian and parameters

The degrees of freedom needed to describe the physics of manganites are[11] the two e_g-like orbitals which make up Mn conduction band: an electrically inert classical core spin representing electrons occupying t_{2g} orbitals at Mn sites and the three even-parity MnO_6 distortion modes Q_0, Q_x, and Q_z. The Hamiltonian for the manganite superlattice is the Hamiltonian for bulk manganites supplemented by Coulombic terms representing the potential arising from the pattern of the La and Sr ions, thus $H=H_{\text{bulk}}+H_{\text{Coul}}$. The bulk Hamiltonian is $H_{\text{bulk}}=H_{\text{band}}+H_{\text{EE}}+H_{\text{Hund}}+H_{\text{el-lat}}+H_{\text{lattice}}$ where

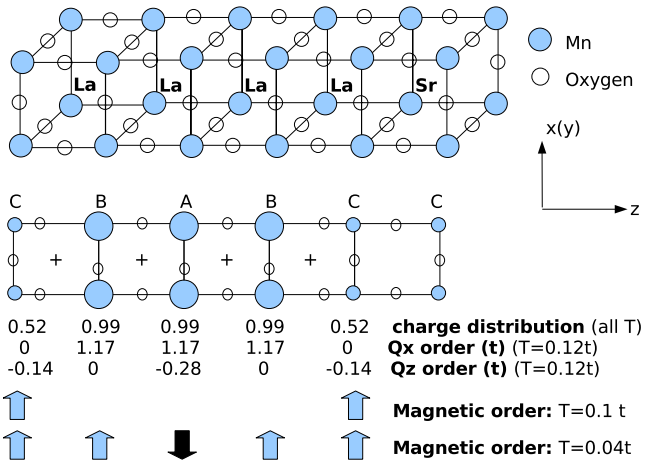

FIG. 1. (Color online) Upper panel: Schematic representation of a $(LaMnO_3)_4$ $(SrMnO_3)_1$ superlattice with Mn manganese and O oxygen ions denoted by shaded and open circles, respectively. Lanthanum and strontium ions labeled by La or Sr reside in the center of cubes defined by Mn. Lower panel: Upper part—projection of (4,1) superlattice onto x-z plane, with the three symmetry inequivalent Mn sites labeled A, B, and C. Middle part—a numerical representation of charge density and amplitude of orbital order computed for screening parameter $\alpha=0.3$ at temperature indicated. Lower part—pictorial representation of magnetic order (order-parameter direction indicated by arrows) calculated using screening parameter $\alpha=0.3$ for two temperatures as indicated.

$$H_{\text{band}} = \sum_{\vec{k},ab,\sigma} \epsilon_{\vec{k},ab,\sigma} c^{\dagger}_{\vec{k},a,\sigma} c_{\vec{k},b,\sigma} \tag{1}$$

with $\epsilon_{\vec{k},ab,\sigma}=-t(\varepsilon_0\hat{e}+\varepsilon_z\hat{\tau}_z+\varepsilon_x\hat{\tau}_x)_{ab}$ where e is the unit matrix, $\hat{\tau}$ are Pauli matrices and $\varepsilon_0=\cos k_x+\cos k_y+\cos k_z$, $\varepsilon_z=\cos k_z-\frac{1}{2}(\cos k_x+\cos k_y)$, and $\varepsilon_x=\frac{\sqrt{3}}{2}(\cos k_x-\cos k_y)$. a,b label orbitals, i,j label sites, and σ labels spins. From our previous band-structure calculation,[18] the hopping parameter t is 0.65 eV which defines the energy unit. We note that the states described by Eq. (1) are Mn-O antibonding, but only the dispersion is relevant here,

$$H_{\text{EE}} = (U-J)n_1n_2 + U\sum_{i=1,2} n_{i,\uparrow}n_{i,\downarrow} + J(c^{\dagger}_{1,\uparrow}c^{\dagger}_{1,\downarrow}c_{2,\downarrow}c_{2,\uparrow} + \text{H.c.}) - 2J\vec{S}_1\cdot\vec{S}_2 \tag{2}$$

with $\vec{S}_{1(2)}=\vec{\sigma}_{\alpha\beta}c^{\dagger}_{1(2),\alpha}c_{1(2),\beta}$. The values $U\sim 2.5$ eV and $J\sim 0.5$ eV are found to be appropriate for the manganite[19]

$$H_{\text{Hund}} = -J_H\sum_i \vec{S}_i\cdot c^{\dagger}_{i,\alpha}\vec{\sigma}_{\alpha\beta}c_{i,\beta} \tag{3}$$

with $J_H\sim 1.5$ eV and $|\vec{S}|=1$. An additional antiferromagnetic core-spin interaction exists in the material. This interaction is crucial for $x>0.5$ but affects only minor details of the $x<0.5$ regime of interest here, i.e., it changes the phase boundaries but does not lose any exhibited phases. Including this interaction involves too great a computational expense, so we do not include it here.

For the electron-lattice interactions[12] we only include the Jahn-Teller coupling,

$$H_{\text{JT}} = -\sum_{i,a,b}(Q_{i,x}\tau^x_{ab}+Q_{i,z}\tau^z_{ab})c^{\dagger}_{i,a}c_{i,b} = -\sum_{i,a,b}\vec{Q}_i\cdot\vec{\tau}_{ab}c^{\dagger}_{i,a}c_{i,b} \tag{4}$$

with $\vec{Q}_i=(Q_{i,x},Q_{i,z})=Q_i(\sin 2\theta_i,\cos 2\theta_i)$ $(0<\theta<\pi)$. We neglect the breathing mode coupling[12] in the current calculation.

For the lattice Hamiltonian we include an elastic energy term from adjacent Mn-O and Mn-Mn force constants[15,20] and the cubic term noted by Kanamori,[21]

$$H_{\text{lattice}} = \sum_{ij,ab}\frac{1}{2K^{ab}_{ij}}Q_{i,a}Q_{j,b} - A\sum_i(3Q^3_{i,z}-Q^2_{i,x}Q_{i,z}), \tag{5}$$

with i,j labeling sites while a,b labeling distortion modes.

As far as e_g electrons are concerned, La and Sr ions act as +1 and neutral point charges, respectively.[22,23] In the superlattice, the distribution of those cations is patterned and the Hamiltonian from electrostatics is

$$H_{\text{Coul}} = \sum_{ij}\left[\frac{1}{2\bar{\epsilon}}\frac{e^2n_in_j}{|\vec{r}_i-\vec{r}_j|} + \frac{1}{2\bar{\epsilon}}\frac{e^2}{|\vec{R}^{\text{La}}_i-\vec{R}^{\text{La}}_j|} - \frac{e^2n_i}{\bar{\epsilon}|\vec{r}_i-\vec{R}^{\text{La}}_j|}\right] \tag{6}$$

with $n_i=\Sigma_{\sigma,a}c^{+}_{i,a,\sigma}c_{i,a,\sigma}$ as the occupation number at Mn site i. $\vec{r}_i$ and $\vec{R}^{\text{La}}_i$ are positions of Mn and La in ith unit cell and $\bar{\epsilon}$ is the dielectric constant of the material. To describe the magnitude of this interaction, we define the dimensionless screening parameter $\alpha\equiv e^2/a\bar{\epsilon}t$ which controls the charge-density distribution. The value of α has not been determined, but its order of magnitude may be estimated from the hopping parameter $t\sim 0.65$ eV, lattice constant $a=4$ Å, and typical value of dielectric constant $\bar{\epsilon}\sim 10$ (Ref. 24) to be $\alpha=0.2$.

C. Method and results from bulk model

We now briefly discuss the method of solving the model. To solve the model we use the single-site dynamical mean-field theory (DMFT) (Ref. 25) with semiclassical impurity solver.[26] The intersite lattice coupling (cooperative Jahn-Teller effect[20,27]) is taken into account within the single-site DMFT by the mean-field approximation, i.e., the local impurity problem contains an effective interaction from distortions at neighboring sites.[15] For the term introduced by the superlattice H_{Coul}, we adopt the Hartree approximation whose overall effect is to generate a self-consistent potential at each Mn site.[22,23] The optical conductivities are computed in the same manner as described in Ref 14 and the dc values are obtained by taking the $\omega\to 0$ limit. Specifics of the DMFT computation are presented in Ref 15.

The first step to study the superlattice is to understand the parental bulk system. Figure 2 shows the theoretically calculated bulk phase diagram. Figure 2 is different from what we presented in Ref 15 in-phase boundaries because here we neglect the AF magnetic coupling between Mn core spins. This simplification does not lose any phases for the doping range $x<0.5$ but does lose phases for $x>0.5$; therefore we only present bulk results for $x<0.5$ and only consider

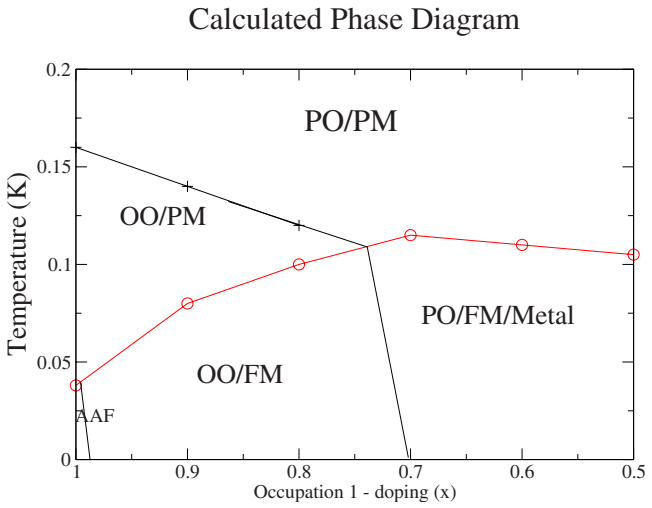

FIG. 2. (Color online) The calculated bulk phase diagrams. To make comparison between our calculations and experiments, the calculation done at $T=0.1t$ corresponds to roughly 250 K in the experiments (Ref. 15).

$[n(\geq 2),1]$ superlattices where all layers have e_g electron occupations larger than 0.5. Our bulk calculation overestimates the transition temperatures but gives a reasonable description of the ordering of phases. For this reason we focus on the exhibited phases in superlattice but not the transition temperatures on the numerical values.

D. Planar long-ranged orders

Similar to earlier findings,[22,23] the superlattice results are most naturally presented by first describing the charge density and exhibited order(s) at each x-y plane and the superlattice phases are therefore the planer phases plus the relations between them. To facilitate later discussion, we summarize here the three planar long-ranged orders found in our calculation: a (π,π) staggered Q_x, a uniform Q_z, and a FM order. The first two are orbital orders; the ordering patterns are shown in Fig. 3. For the staggered Q_x order, all octahedra in the plane undergo Q_x distortions with the long axis of each distorted octahedron differs by 90° from its adjacent ones, as shown in Fig. 3(a). For the $+(-)Q_z$ order, all oxygens are in the middle of neighboring Mn, but the Mn-O distance in the z direction is longer(shorter) than that in x and y, as shown in Fig. 3(b).

An equivalent way to describe the local-orbital order is to use the ground state $|\theta\rangle=\cos\theta|3z^2-r^2\rangle+\sin\theta|x^2-y^2\rangle$ (Ref. 15) of the Jahn-Teller coupling [Eq. (4)] with $\vec{Q}_i$ given by the distortions. In this language the (π,π) Q_x order corresponds to an alternating $|\theta=\pi/4\rangle$, $|\theta=-\pi/4\rangle$ corresponds to the orbital configuration, and the uniform $+(-)Q_z$ corresponds to a uniform $|\theta=0\rangle$ ($|\theta=\pi/2\rangle$).

III. RESULTS FOR (4,1) SUPERLATTICE

In this section we present our calculated results for the (4,1) superlattice: a representative case that captures most of the relevant phenomena. We consider two different values of

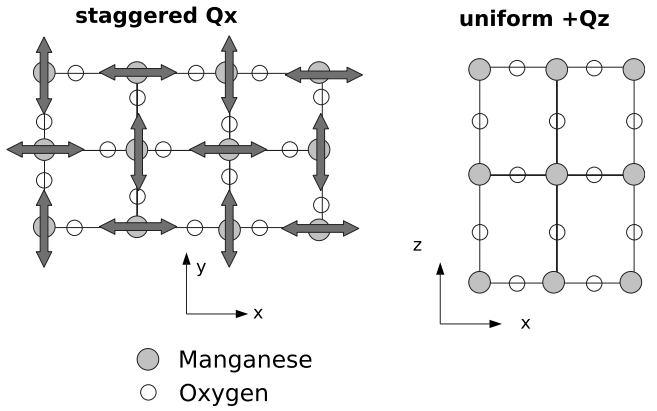

FIG. 3. The orbital orders. (a) The staggered Q_x and (b) uniform Q_z orders. For the staggered Q_x order, all octahedra in the plane undergo Q_x distortions with the long axis (double arrows) of each distorted octahedron differs by 90° from its adjacent sites. For the $+(-)Q_z$ order, all oxygens are in the middle of neighboring Mn, but the Mn-O distance in z direction is longer (shorter) than that in x and y.

α; $\alpha=0.09$ corresponding to relatively delocalized electrons and $\alpha=0.3$ corresponding to tightly confined electrons.

For L4S1 each supercell has three symmetry-inequivalent layers labeled as A, B, and C, as illustrated in Fig. 1(b). Figure 4 presents the L4S1 layer charge distribution for $\alpha=0.09$ (corresponding to a relatively delocalized electrons) at temperatures $0.16t$ (above any ordered temperatures), $0.12t$ (orbital ordering but not magnetic ordering presented), and $0.04t$ (both orbital and magnetic orders). The variation in charge distribution for different temperatures is smaller than 5%. We note that very recent x-ray scattering experiments on manganite superlattice[28] indicate a large change in L and K edge absorption intensities as the temperature is decreased through the Curie temperature. If the experiments measure the total interface charge density, they may be in contradiction to our results, but if data are proportional to the near-Fermi-surface coherent excitations (which grow below Curie temperature according to our calculation), there may not be a contradiction.[29]

The staggered Q_x order. Table I lists the layer charge density, the computed SL Q_x order, and the bulk Q_x order at the given layer charge density of the (4,1) SL for $\alpha=0.3$ and

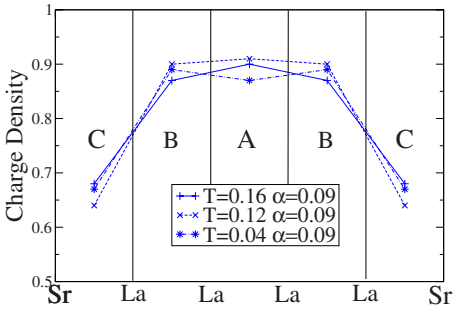

FIG. 4. (Color online) L4S1 charge distribution for $\alpha=0.09$ at $0.16t$ (above any ordering temperatures), $0.12t$ (orbital ordering but not magnetic ordering in superlattices), and $0.04t$ (both orbital and magnetic orders presented).

TABLE I. The amplitudes of the staggered Q_x ($|\langle Q_x^s \rangle|$) and uniform Q_z ($|\langle Q_z^u \rangle|$) orders for the L4S1 superlattice and for the corresponding bulk values at same densities for $T=0.12t$.

	$\alpha=0.3$			$\alpha=0.09$		
Site label	A	B	C	A	B	C
Charge density	0.99	0.99	0.52	0.92	0.90	0.64
$\|\langle Q_x^s \rangle\|$ SL [t]	1.17	1.17	0	1.01	1.0	0
$\|\langle Q_x^s \rangle\|$ Bulk [t]	1.18	1.18	0	1.02	1.0	0
$\|\langle Q_z^u \rangle\|$ SL [t]	−0.28	0	−0.14	−0.18	−0.03	−0.08
$\|\langle Q_z^u \rangle\|$ Bulk [t]	−0.32	−0.32	0	−0.22	−0.2	0

0.09 at $T=0.12t$. We see that the SL calculation is very close to the bulk (<1%) which means that the Q_x order is mainly determined by its layer charge density and the proximity effect is very weak.

The very weak orbital order proximity effect for the staggered Q_x order has a straightforward physical origin. Rotation symmetry about the bond in the z direction means that neither nearest-neighbor (NN) hopping nor nearest-neighbor atom-atom forces can distinguish $+Q_x$ order from $-Q_x$ order. One consequence is that within this approximation (π,π,π) Q_x and $(\pi,\pi,0)$ Q_x orders are degenerate implying that the in-plane (π,π) Q_x order does not have any dispersion in z direction and thus no interlayer coupling (no proximity effect) for this order. Second-neighbor hopping[15] or certain classes of shear elastic forces[30] do distinguish the two but the differences are small (of the order of minielectron volt). We will give a more detailed discussion in Sec. V C.

The uniform Q_z order. The third and fourth rows in Table I list the computed SL Q_z order (reflective of the uniform strain in the superlattice) of the (4,1) SL for $\alpha=0.3$ and 0.09 at $T=0.12t$ and the corresponding bulk results at the same density. These results can be understood as follows. There are two apparent sources affecting the uniform Q_z order—the anharmonic term in H_{lattice} and the SL effect. The net SL effect is to produce an electrostaticlike force, i.e., oxygens are pushed toward Mn layer with less e_g density. One must bear in mind that the origin of this force is because the octahedral distortion changes the Mn-O hybridization thus it affects the population distribution of e_g orbitals and has little to do with the actual static Coulomb energy.[15] For the parameters considered above, layer A is sandwiched by layer B having similar charge densities (one in this case); therefore the SL effect is weak for A and the main contribution is from the anharmonic effect. Indeed the Q_z order of layer A is $-0.28t$, which is very close to the bulk result $-0.32t$. For layer B, besides the bulk effect which causes a $-Q_z$ order, the charge inhomogeneity results in a $+Q_z$ order since oxygens are pushed *away* from layer B and in this case these two effects nearly cancel each other. For layer C, only the SL effect contributes and the result is a $0.14t-Q_z$ order. We see that at interfaces the bulk and SL effects are of comparable strengths; therefore the uniform Q_z order has a significant proximity effect.

The magnetic order. Now we discuss the magnetic order for $\alpha=0.3$ and 0.09. For $\alpha=0.3$, only layer C has FM order at $T=0.1t$. When lowering the temperature to $0.04t$, all layers are two-dimensional (2D) FM. The interlayer coupling between A and B (with layer densities roughly one) is AF and all others are FM as shown in Fig. 1(b). For $\alpha=0.09$, one obtains a smoother charge distribution and at low-temperature all interlayer magnetic couplings are FM. Those results suggest that the interlayer magnetic coupling is generally ferromagnetic except that between layers with densities close to one. The FM coupling between layers can be understood from double-exchange mechanism where FM arrangement maximizes the kinetic energy and is energy favored when the conduction band is not full. The AF coupling between $N=1$ layers has the same origin as the bulk[15] where the system gains gap energy by arranging core spins antiferromagnetically. One interesting consequence of these results is that if the charge density is sufficiently sharp enough to introduce AF interlayer coupling ($\alpha=0.3$, for example), the superstructures with odd number of La have an odd number of AF bonds so the magnetic lattice has twice the period of the structured one. For example, for the L3S1 superlattice, we expect the period including the magnetic order is eight and adding up magnetic orders from all layer leads to zero total magnetization.

IV. SPECTRAL FUNCTIONS AND CONDUCTIVITIES FOR DIFFERENT SUPERLATTICES

In this section we shall first establish the rule implied from our superlattice calculation for the in-plane conductivity and also discuss the out of plane one. Based on the established rule we discuss the temperature and superlattice dependences on the dc measurements.

A. Rule for the conductivity

We found that once the layer charge densities n_i are specified, the excitation spectrum at each layer behaves very close to the bulk at the same density. We use the simplest superlattice L2S1 to demonstrate this point. For (2,1) SL there are only two symmetry-inequivalent sites: one between La labeled as A while the other between La and Sr B, as shown in Fig. 5(a). For $\alpha=0.3$ and $T=0.12t$ we found $n_A\sim 1$ and $n_B\sim 0.5$. Figures 5(a) and 5(b) show both the calculated SL spectral functions for layer B(A) and the bulk for $N=0.5(N=1)$ at the same temperature.

Since the in-plane conductivity σ_{xx}^{SL} is dominated by in-plane hopping processes (moving electrons from one site to

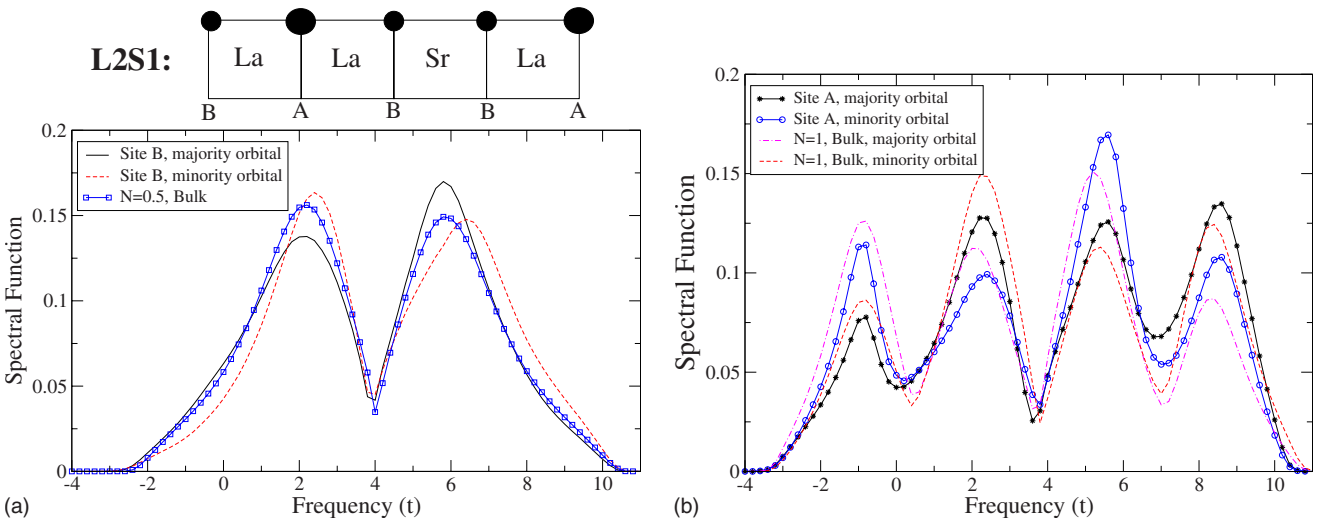

FIG. 5. (Color online) Spectral functions for the (2,1) superlattice compared to bulk spectra at density equal to layer density for $\alpha=0.3$ and at $T=0.12t$. (a) The superlattice spectral functions for layer B and bulk at $N=0.5$. (b) SL spectral functions for layer A and bulk at $N=1$. To facilitate the comparison, the bulk results are shifted $0.4t$ in frequency. The peak-peak distances are essentially the same for bulk and SL calculations.

the other within the same layer) *and* the spectral function for layer with density n_i is very close to the bulk at the same density, $\sigma_{xx}^{\mathrm{SL}}$ should be very close to the bulk-averaged value $\bar{\sigma}_{xx}^{\mathrm{bulk}}$ which is define as

$$\bar{\sigma}_{xx}^{\mathrm{bulk}} \equiv \sum_{i=1}^{N} \sigma_{xx}^{\mathrm{bulk}}(n_i)/N. \tag{7}$$

To see how accurate this rule is, we list in Table II the calculated SL dc conductivity $\sigma_{xx}^{\mathrm{SL}}$ and the bulk averaged $\bar{\sigma}_{xx}^{\mathrm{bulk}}$ according to the obtained charge distribution at $T=0.12t$ where the unit for σ_{xx} is $e^2/(\hbar a)\sim 6\times 10^3(\Omega\ \mathrm{cm})^{-1}$ with a as the lattice constant (~ 4 Å). As a concrete example we compute bulk averaged $\bar{\sigma}_{xx}^{\mathrm{bulk}}$ for L4S1, $\alpha=0.09$, and $T=0.12t$ in details. From Fig. 4 we see that there are two layers with density 0.9 (layer B), two layers with 0.64 (layer C), and one layer with density 0.91 (layer A) for those parameters. Now we consult the bulk results for dc conductivity at $T=0.12t$ and find that $\sigma_{xx}^{\mathrm{bulk}}$ at $N=0.9$, 0.64, and 0.91 are 0.055, 0.12, and 0.05, respectively. The bulk averaged $\bar{\sigma}_{xx}^{\mathrm{bulk}}$ is thus $[2\sigma_{xx}^{\mathrm{bulk}}(n=0.9)+2\sigma_{xx}^{\mathrm{bulk}}(n=0.64)+\sigma_{xx}^{\mathrm{bulk}}(n=0.91)]/5$ roughly 0.081. As listed in Table II, the difference between $\bar{\sigma}^{\mathrm{bulk}}$ and $\sigma_{xx}^{\mathrm{SL}}$ is roughly 10% for L2S1 and is smaller ($\sim 2\%$) for L3S1 and L4S1. Figure 6 compares the in-plane optical conductivities with the bulk averaged for the L4S1 at $\alpha=0.3$ and $T=0.12$. We see that they match quite well ($\lesssim 10\%$) (both peak positions and peak amplitudes) for all frequencies.

TABLE II. $\sigma_{xx}^{\mathrm{SL}}$ and $\bar{\sigma}_{xx}^{\mathrm{bulk}}$ for different superlattices.

α	0.3	0.09	0.3	0.09	0.3	0.09
$\bar{\sigma}_{xx}^{\mathrm{bulk}}$	0.083	0.115	0.064	0.093	0.58	0.082
$\sigma_{xx}^{\mathrm{SL}}$	0.077	0.105	0.067	0.093	0.6	0.081
SL	L2S1	L2S1	L3S1	L3S1	L4S1	L4S1

Unlike the in-plane case, the out-of-plane conductivity $\sigma_{zz}^{\mathrm{SL}}$ involves interlayer hopping processes (removing electrons from layer i and adding them to layer $i\pm\hat{z}$). Since different layers experience different static Coulomb potential, there is no simple relation between $\sigma_{zz}^{\mathrm{SL}}$ and $\{n_i\}$. Our previous study[22] of a simpler model system, namely, the one-orbital double-exchange superlattice, shows that there are peaks in $\sigma_{zz}^{\mathrm{SL}}(\omega)$ directly corresponding to the potential difference between layers from which the α is determined straightforwardly. However for the current problem the potential difference is mainly to produce layer-dependent local spectra and are not directly related to peaks in $\sigma_{zz}^{\mathrm{SL}}$. Nonetheless $\sigma_{zz}^{\mathrm{SL}}$ is more sensitive to the screening parameter than $\sigma_{xx}^{\mathrm{SL}}$ and can be used to constrain the values of α. We will return to this point in Sec. V B.

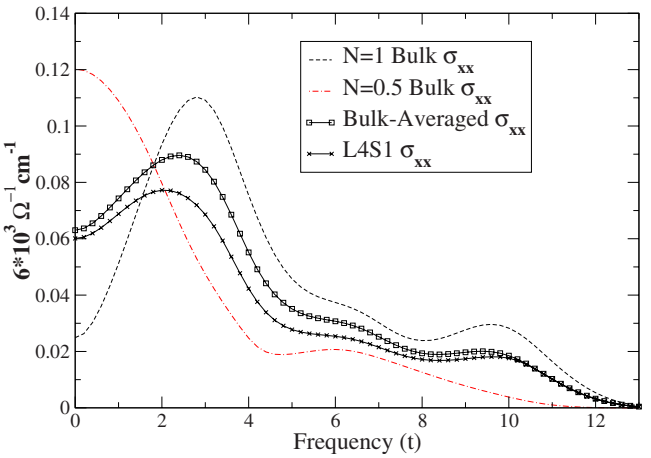

FIG. 6. (Color online) Calculated SL in-plane optical conductivity and the corresponding bulk averaged one for the L4S1 at $\alpha=0.3$ and $T=0.12t$. As a reference we also plot the bulk $\sigma_{xx}(\omega)$ for $N=1$ and 0.5 (curves without ligands) at the same temperature which are used for computing the bulk-averaged conductivities.

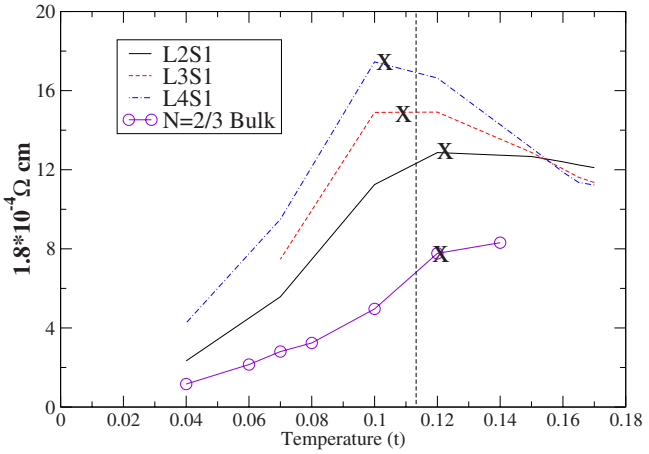

FIG. 7. (Color online) The dc resistivity as a function of temperature for $\alpha=0.3$. *X* indicates the calculated interface Curie temperature for each superlattice. The vertical dashed line marks a rough temperature where $d\rho/dT$ changes sign. As a reference we also present the bulk result for $N=2/3$ ($x=1/3$).

B. Temperature dependence of dc resistivity

Now we discuss the temperature dependence on the dc resistivity ρ. Figure 7 shows $\rho(T)$ for $\alpha=0.3$. We observe that around $T=0.11t$ $d\rho/dT$ changes sign implying the superlattice goes from high-T insulating phase to low-T metallic. This *downturn* in $\rho(T)$ coincides with the interface Curie temperatures which are also marked [Fig. 7]. Across this temperature the interfaces go from paramagnetic (PM) or bad metal to FM or metal accounting for the superlattice metallic behavior. From double-exchange mechanism,[14,15] the PM or FM transition is always accompanied with an insulator or metal (bad metal or metal at least) transition; the sign change in $d\rho/dT$ as a function of temperature is quite general for all values of α, but is more pronounced for large α.

C. Superlattice dependence of dc conductivity

Since for small α, the superlattice behaves just like the bulk material, we only focus on the α which leads to the sharp charge distribution, i.e., $\alpha=0.3$. Our result implies that the SL conductivity is proportional to the interface density at low temperature (the interface density is defined as the ratio between the numbers of Mn sandwiched by La *and* Sr and that of total Mn layers; for L2S1 the interface density is 2/3 and for L4S1 the interface density is 2/5). This statement is a direct consequence of the rule $\sigma_{xx}^{\mathrm{SL}} \sim \bar{\sigma}_{xx}^{\mathrm{bulk}}$: for sharp charge distribution, $N\sim 1$ layers are insulating at low T and only interface layers ($N\sim 0.5$) are conducting. To demonstrate this statement from the SL calculation, we define $r(T)=\sigma_{xx}^{\mathrm{L4S1}}(T)/\sigma_{xx}^{\mathrm{L2S1}}(T)$ and compare it with the ratio of interface densities between L4S1 and L2S1 which is 0.6. The following table presents $r(T)$ for several temperatures:

T/t	0.15	0.1	0.07	0.04
$r(T)^{\alpha=0.3}$	0.96	0.65	0.55	0.57

We see that $r(T)$ is indeed very close to 0.6 below the interface Curie temperature ($\sim 0.11t$). Finally we emphasize that from our calculation, the statement "SL conductivities are only from interfaces" is true only below temperature *and* with sharp charge distribution.

V. DISCUSSION

In this section we first summarize our results by providing rules deduced from our calculations then we discuss how to determine the layer charge distribution and thus the screening parameter experimentally. Finally we give a more detailed analysis on the proximity effect of the orbital orders.

A. Rules implied by the calculation

The exhibited phases at each layer are the combined effects of bulk Hamiltonian and the charge inhomogeneity induced by the SL. Here we summarize our calculations by stating the following rules which govern the displayed phases at each layer.

(1.) *The charge distribution* is mainly determined by the screening parameter α and is not sensitive to the temperatures and orders.[22,23]

(2.) *The staggered Q_x order* at each layer follows the bulk behavior at the corresponding layer charge density.

(3.) *The uniform Q_z order* is caused by two sources. First (bulk effect), a uniform $-Q_z$ order is induced with the presence of the staggered Q_x order. Second (SL effect), the charge inhomogeneity induces an electrostaticlike force pushing oxygens closer to the layer with lower density. Note that the origin of this force is the Mn-O antibonding.[15]

(4.) *The magnetic order*: The interlayer coupling is FM except that between layers with densities close to one.

(5.) *The in-plane conductivity* of the SL is essentially the average of the bulk conductivities, i.e., for a given charge distribution $\{n_1,n_2,..n_N\}$, $\sigma_{xx}^{\mathrm{SL}}=\bar{\sigma}_{xx}^{\mathrm{bulk}}=\Sigma_{i=1}^{N}\sigma_{xx}^{\mathrm{bulk}}(n_i)/N$ while we do not have a simple rule for out-of-plane conductivities.

B. Determining the charge distribution and screening parameter

Our results indicate that the key quantity for the SL is the charge distribution and therefore determining the screening parameter α is very important. In principle the charge distribution can be determined by measuring the change in manganese valence in the superlattice,[1] but such measurements have not to our knowledge been performed on manganite superlattices. Here we propose two measurements to constrain the values of α. The first proposal is to grow superlattices with odd number of $LaMnO_3$ layers (L3S1, for example) and to measure the total magnetization at low temperature. If the charge distribution is sharp then the ferromagnetic interface layers are antiferromagnetically coupled and the layer has zero net magnetization; whereas if the charge distribution is broad, the system will simply be ferromagnetic. This method suffers from a potential experimental disadvantage: Lack of perfect oxygen stoichiometry could produce ferromagnetism in the La-rich regions even in the presence of a sharp charge distribution.[4,31]

The second one is to measure the optical conductivity. The basic idea is that one should be able to decompose the

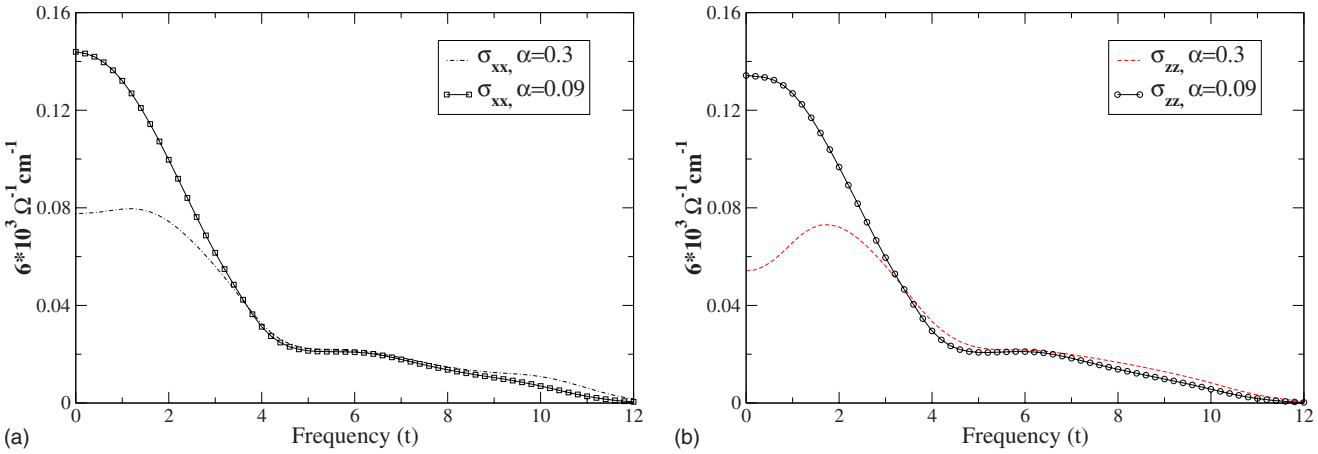

FIG. 8. (Color online) (a) In-plane and (b) out-of-plane optical conductivities for L2S1 for $\alpha=0.09$ (with ligands) and 0.3 (without ligands) at $T=0.12t$.

in-plane optical conductivities into sum of bulk results. This measurement is free from the interferences of the impurity scattering or extra oxygens in the superlattice. Figure 8(a) shows the in-plane L2S1 optical conductivities $\sigma_{xx}^{\mathrm{L2S1}}(\omega)$ for $\alpha=0.3$ and $\alpha=0.09$ at $T=0.12t$ ($\sim$300 K and with interfaces being slightly ferromagnetic). We see that for $\alpha=0.3$, the $\sigma_{xx}^{\mathrm{L2S1}}(\omega)$ is not peaked at zero frequency because 1/3 of the contribution is from Mn layers with density close to one. On the other hand for $\alpha=0.09$, $\sigma_{xx}^{\mathrm{L2S1}}(\omega)$ behaves more like a bulk material.

The out-of-plane conductivities contain information of the potential differences at different layers. As discussed in Sec. IV A, as far as the σ_{zz} is concerned, the main effect of the layer-dependent potentials is to produce layer-dependent local spectral functions which makes σ_{zz} different from σ_{xx} at high-T nonordered phase. Therefore the anisotropy in σ above ordering temperatures is a very straightforward estimator of how confined or delocalized the electrons are. Figure 8(b) shows the out-of-plane conductivity $\sigma_{zz}^{\mathrm{L2S1}}(\omega)$ for the (2,1) superlattice. As expected larger α results in larger anisotropy in σ. For the numerics, because the potential difference is not directly related to the peak in the out-of-plane optical conductivity as in the model studied in Ref 22, one has to compare the experimental data with theoretical results.

C. Orbital order proximity effects

Our calculation indicates that orbital order associated with the Q_z mode (octahedral distortion with long bond pointing along z direction) is reasonably efficiently transmitted from one layer to the next; whereas orbital order associated with Q_x (octahedral distortion with long axis in x-y plane) is not transmitted at all. The approximations made in this paper amount to retaining only nearest-neighbor interactions in both the electronic and lattice sectors; in this approximation rotational invariance about the bond in the z direction ensures that Q_x order is not transmitted. In this section we estimate the extent to which terms not included in our model may change this result.

The transmission of Q_x orbital order implies an energy difference between states in which Mn ions in adjacent planes have the same or opposite amplitudes for Q_x order. To estimate this we consider the energy difference between $(\pi,\pi,0)$ and (π,π,π) orbital order. There are two contributions to this energy: electronic and elastic.

We begin with the electronic term. A given lattice distortion selects one locally favored state of each site i, which we refer to as $|\theta_i^g\rangle=\cos\theta_i|3z^2-r^2\rangle+\sin\theta_i|x^2-y^2\rangle$ and also the orthogonal excited state $|\theta_i^e\rangle$. For the $+Q_x$ distortion the locally favored state is $|\theta_{Q_x}^g\rangle=\frac{1}{\sqrt{2}}|3z^2-r^2\rangle+\frac{1}{\sqrt{2}}|x^2-y^2\rangle$ and the locally disfavored state is $|\theta_{Q_x}^e\rangle=\frac{1}{\sqrt{2}}|3z^2-r^2\rangle-\frac{1}{\sqrt{2}}|x^2-y^2\rangle$; for the $-Q_x$ distortion the roles of θ^g and θ^e are reversed.

The $(\pi,\pi,0)$ Q_x and (π,π,π) Q_x orders produce exactly the same local distortions; an electronic contribution to the energy difference between these two orders can therefore only arise from a difference in the electronic hybridization energies for the two states. We now argue that if only nearest-neighbor hopping is present, there can be no hybridization energy difference between the two states. The in-plane hopping is trivially the same for the two states; a difference can therefore only arise from the z-direction hopping. The hybridization is given by a 2×2 matrix; in the nearest-neighbor hopping approximation the matrix is degenerate in all three directions with only one nonzero eigenvalue t. For hopping in the z direction the only nonvanishing matrix element is the one connecting $|3z^2-r^2\rangle$ orbitals on the two sites implying that the matrix element between any combination of $|\theta_{Q_x}^g\rangle$ and $|\theta_{Q_x}^e\rangle$ is $t/2$, so that the nearest-neighbor hopping does not distinguish between the two states. Including the second NN couplings can lift this degeneracy. The energy difference can be estimated by comparing the energy gain caused by the virtual processes involving second NN hoppings (superexchange) and is done in Ref 15. The local-density approximation (LDA) calculation[18] suggests the second NN hopping is roughly 0.035 eV, leading to an energy difference of the order of minielectron volt for these two orders.

We next consider contributions arising from elastic forces. In a ball and spring model, we have found that oxygen-oxygen or three-body forces are required to propagate Q_x order. For these situations, spring constant models are not

reliable and band theory calculations of phonon stiffness are required. Available information on these forces is presented in Ref. 30; the result is that the energy difference is of the order of minielectron volt, roughly the same magnitudes as the electronic contribution. With these estimates we conclude that our model captures the main physics of manganites and the proximity effect for the planar staggered Q_x order is indeed very weak in reality.

VI. CONNECTIONS TO EXPERIMENTS

The temperature dependences of the dc resistivity (ρ) and magnetization (M) of $(LaMnO_3)_{2n}(SrMnO_3)_n$ [the $(2n,n)$ superlattice in our notation] have been measured.[4,5] In this section we discuss the connection between our calculation and these measurements.

A. dc resistivity

For the resistivity measurement, as the temperature is decreased from 400 K, the resistivity ρ is found to increase until a superlattice-dependent temperature T_d is reached. This "downturn" in $\rho(T)$ is observed for all $(2n,n)$ superlattices. The temperature at which the downturn occurs (T_d) is n dependent (larger n lower T_d) and is roughly 200–350 K [Figs. 2(a)–2(c) in Ref. 4 and Fig. 2 in Ref. 5]. Above T_d, the magnitude of ρ has a very strong dependence on n. When the temperature is further reduced below 100 K, the resistivity increases again for $n>3$ superlattice while it keeps on decreasing for $n<3$.

Calculation finds two typical behaviors corresponding to weakly and strongly bound charge distributions. For both cases we expect a downturn in resistivity which is associated with the interface FM or PM transition with the downturn temperature essentially n independent. At very low temperature our theory predicts metallic ($d\rho/dT>0$) behavior. The n dependence on the magnitude of ρ is different for these two limits: for the weakly bound charge distribution ρ has very weak n dependence while for the strongly bound ρ is proportional to the interface density and thus $\propto n$.

The results according to our rules are in reasonable agreement with the $n<3$ superlattices because they remain metallic in the low temperature. For long period superlattice, except the existence of the changing sign in $d\rho/dT$, our theory is not compatible with experiments at quantitative level because of the exhibited n dependence on ρ and T_d and because of the low-T insulating phase. Essentially the experimental measured ρ depends too strongly on n compared to our theoretical prediction as shown in Fig. 9. We think these inconsistencies are caused by the n-dependent interface quality.

B. Magnetization

For the magnetization measurement, Ref. 4 [Figs. 2(d)–2(f)] shows that all superlattices exhibit a net magnetization below some onset temperature T_c^I (the superscript I denotes interface). T_c^I depends on n (decrease in T_c^I from 300 to 200 K when increasing n from 2 to 16) and is very close to the downturn temperature in resistivity T_d. For the $n=2$ superlattice, the magnetization increases and saturates when

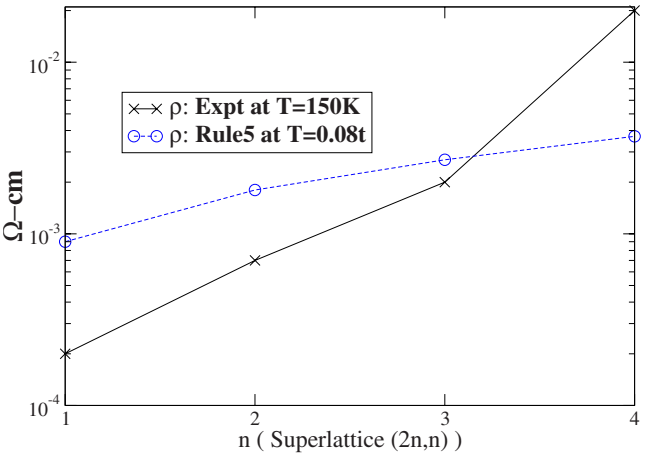

FIG. 9. (Color online) The in-plane dc resistivities from experiment at $T=150$ K (Ref. 5) (solid line) and from rule 5 at $T=0.08t$ with sharp charge distribution.

lowering the temperature. For $n=4$ and 16 superlattices, the magnetization increases slowly right below T_c^I then more rapidly around 150 K. When the system is further cooled without applying a magnetic field [zero-field cooling (ZFC)], the magnetization reaches a maximum (roughly the same value $\sim 0.4\mu_B$/Mn for both $n=4$ and 16) around 110 K, before it eventually decays to zero. If the system is cooled in an applied magnetic field [field cooling (FC)], the $n=2$ superlattice behavior is not changed but for both $n=4$ and 16 the magnetization saturates at $0.6\mu_B$/Mn approaching zero temperature. We believe that the FC measurements reveal more clearly the intrinsic behavior and we will therefore focus on the FC data but we will comment on the ZFC data in the end.

Our calculation predicts that ferromagnetism is associated with the interfaces. There is a critical thickness which depends on the width of the charge distribution (value of α). For systems with n greater than this critical value (which may be zero for very sharp charge distributions), the magnetization resides only on the interfaces, so one expects an onset at the interface T_c (comparable to the bulk value) and a saturation value scaling with the interface density (with coefficient depending on α).

Now we discuss the magnetization (the FC data) based on our calculation. First our theory agrees reasonably well with the $n=2$ (L4S2) superlattice assuming the critical thickness is $\gtrsim 3$ so the $LaMnO_3$ layers are ferromagnetically ordered (the $n=2$ superlattice saturates at $2.8\mu_B$/Mn at low temperature indicating $LaMnO_3$ layers are ferromagnetic). However, the behavior of the $n=4$ and 16 superlattices is not consistent with our theory, except in the qualitative sense that resistivity downturn and magnetic-onset temperatures coincide. The strong n dependence of the magnetism-onset temperature T_c^I is not found in the calculation, where ferromagnetism is an interface phenomenon and therefore not strongly n dependent. Further, the observed rapid growth in M below 140 K and the saturation at about $1\mu_B$ displayed in the long period $(n>6)$ superlattices is not found in our theory, which instead implies *antiferromagnetism* below 140 K and a saturation magnetization proportional to the interface density.

We believe that the inconsistency is a consequence of oxygen stoichiometry that extra oxygens reside in La-riched

regions so that $LaMnO_3$ is effectively a slightly doped manganites.[4,31] Based on this assumption and our rules, we now explain the FC data. Our rule states that each layer behaves as a bulk manganite at the given charge density. For the density close to but not equal to one, the system displays canted A-AF order[11] around 140 K which has a small but nonzero net magnetic moment. Within this picture, the constant but small saturation magnetization for $n>6$ superlattices is the net magnetization from the canted A-AF order and the rapid growth around 140 K which is caused by the forming of the canted A-AF order in the La-riched regions. The remaining issue is the n dependence on the interface Curie temperature. We believe this is caused by the n-dependent interface quality. Since the main energy gain for PM or FM transition is the kinetic energy (double exchange), we expect the bad interface quality tending to localize electrons will reduce the Curie temperature. This is qualitatively consistent with the observation.

Finally we comment on the zero-field-cooled data. The most striking feature for ZFC data is that for the $n \geq 4$ superlattice the magnetization starts to decrease around 110 K upon cooling. We associate this reduction in M with the G-AF order developed in the $SrMnO_3$ layers. The forming of G-AF order in $SrMnO_3$ weakens or temporarily kills the ferromagnetic coupling between ferromagnetic interfaces, therefore it reduces the total magnetization. Note that the Neel temperature for $CaMnO_3$ is 110 K.[16]

C. Interface qualities and proposed experiments

Although the qualitative interpretations can be made, our rules are not compatible with experimental data at quantitative level, in particular, the resistivity measurement. We believe this discrepancy is mainly caused by the n-dependent interface quality which has two possible causes. The first one is the mismatch in lattice constant. Since the $LaMnO_3$ and $SrMnO_3$ have slightly different lattice constants, the interface either tolerates very large strain forces or more probably creates some defects to compensate the mismatch. The presence of defects increases the scattering sources and thus the resistivity which is not considered in our model. The second one is the magnetic frustration. Since $LaMnO_3$, $SrMnO_3$ at low temperature displays A-type and G-type AF orders, respectively; interfaces undergo the magnetic frustration which suppresses the tendency of FM order and again increases the resistivity.

To reduce these extra variables in experiments, we propose one should conduct experiments on $(n,1)$ SL. For this $(n,1)$ series SL, since no Mn is sandwiched by Sr layers we expect the effects due to the lattice-constant mismatch should be relatively small. Perhaps more importantly complications from the magnetic frustration caused by $SrMnO_3$ AFM regions will not enter the problem. Based on these arguments the n-dependent interface quality is expected to be strongly reduced and the direct comparison between experiments and theory becomes easier.

VII. CONCLUSION

We have studied the $(LaMnO_3)_n(SrMnO_3)_1$ $(n,1)$ superlattice. We found that the charge distribution determined by the screening parameter α is the key quantity and propose that the optical conductivity measurement of L2S1 can fix it. Once the charge density at each layer is known, the phases essentially follow the bulk at the corresponding density. General rules for phases are given. We propose that measurements on the low-temperature magnetization of the L3S1 SL and on the optical conductivity help constrain the range of α. For $\alpha=0.3$, which results in sharp charge distribution, we predict that at low temperature the $(n,1)$ superlattice has no net magnetization with period $2\times(n+1)$ for odd n. Finally we comment on recent experiments based on our calculations and infer that the main discrepancy is caused by the sample-dependent interface quality. We suggest the $(n,1)$ superlattice is actually a physically simpler and cleaner system to study.

ACKNOWLEDGMENTS

We acknowledge support from DOE under Grant No. ER46189 and the Columbia MRSEC.

[1] M. Ohtomo, D. Muller, D. Grezul, and H. Hwang, Nature (London) **419**, 378 (2002).
[2] J. Chakhalian, J. W. Freeland, G. Srajer, J. Strempfer, G. Khaliullin, J. C. Cezar, T. Charlton, R. Dalgliesh, C. Bernhard, G. Cristiani, H.-U. Habermeier, and B. Keimer, Nat. Phys. **2**, 244 (2006).
[3] A. Brinkman, M. Huijben1, M. van Zalk1, J. Huijben, U. Zeitler, J. C. Maan, W. G. van der Wiel, G. Rijnders1, D. H. A. Blank1, and H. Hilgenkamp, Nature Mater. **6**, 493 (2007).
[4] C. Adamo, K. Xe, P. Schiffer, A. Soukiassian, M. Warusawithana, L. Maritato, and D. G. Schlom, Appl. Phys. Lett. **92**, 112508 (2008).
[5] A. Bhattacharya, S. J. May, S. G. E. te Velthuis, M. Warusawithana, X. Zhai, Bin Jiang, J. M. Zuo, M. R. Fitzsimmons, S. D. Bader, and J. N. Eckstein, Phys. Rev. Lett. **100**, 257203 (2008).
[6] A. Bhattacharya, X. Zhai, M. Warusawithana, J. N. Eckstein, and S. D. Bader, Appl. Phys. Lett. **90**, 222503 (2007).
[7] *The Quantum Hall Effect*, edited by R. E. Prange and S. G. Girvin (Springer-Verlag, Berlin, 1987).
[8] *Quantum Hall Effect*, edited by M. Stone (World Scientific, Singapore, 1992).
[9] M. Imada, A. Fujimori, and Y. Tokura, Rev. Mod. Phys. **70**, 1039 (1998).
[10] J. B. Goodenough, Phys. Rev. **100**, 564 (1955).
[11] *Colossal Magnetoresistive Oxides*, edited by Y. Tokura (Gordon and Breach, New York, 2000).
[12] A. J. Millis, R. Mueller, and B. I. Shraiman, Phys. Rev. B **54**, 5389 (1996); **54**, 5405 (1996).
[13] K. H. Ahn and A. J. Millis, Phys. Rev. B **61**, 13545 (2000).

[14] B. Michaelis and A. J. Millis, Phys. Rev. B **68**, 115111 (2003).
[15] C. W. Lin and A. J. Millis, arXiv:0808.0736 (unpublished).
[16] E. O. Wollan and W. C. Koehler, Phys. Rev. **100**, 545 (1955).
[17] P. Schiffer, A. P. Ramirez, W. Bao, and S.-W. Cheong, Phys. Rev. Lett. **75**, 3336 (1995).
[18] C. Ederer, C. W. Lin, and A. J. Millis, Phys. Rev. B **76**, 155105 (2007).
[19] C. W. Lin and A. J. Millis, arXiv:0808.0733 (unpublished).
[20] A. J. Millis, Phys. Rev. B **53**, 8434 (1996).
[21] J. Kanamori, J. Appl. Phys. **31**, S14 (1960).
[22] C. W. Lin, S. Okamoto, and A. J. Millis, Phys. Rev. B **73**, 041104(R) (2006).
[23] S. Okamoto and A. Millis, Nature (London) **428**, 630 (2004).
[24] S. Okamoto, A. J. Millis, and N. A. Spaldin, Phys. Rev. Lett. **97**, 056802 (2006).
[25] A. Georges, B. G. Kotliar, W. Krauth, and M. J. Rozenberg, Rev. Mod. Phys. **68**, 13 (1996).
[26] S. Okamoto, A. Fuhrmann, A. Comanac, and A. J. Millis, Phys. Rev. B **71**, 235113 (2005).
[27] B. Halperin and R. Englman, Phys. Rev. B **3**, 1698 (1971).
[28] S. Smadici, P. Abbamonte, A. Bhattacharya, X. Zhai, B. Jiang, A. Rusydi, J. N. Eckstein, S. D. Bader, and J. M. Zuo, Phys. Rev. Lett. **99**, 196404 (2007).
[29] S. Okamoto and A. J. Millis, Phys. Rev. B **70**, 241104(R) (2004).
[30] K. H. Ahn and A. J. Millis, Phys. Rev. B **64**, 115103 (2001).
[31] Q. Huang, A. Santoro, J. W. Lynn, R. W. Erwin, J. A. Borchers, J. L. Peng, and R. L. Greene, Phys. Rev. B **55**, 14987 (1997).